Batteries & Supercaps

Research Article
doi.org/10.1002/batt.202200380

Chemistry Europe
European Chemical Societies Publishing

www.batteries-supercaps.org

Smart Multi-Layer Architecture Electrodes for High Energy Density Lithium-Ion Capacitors

Sang Ho Lee*[a]

Multi-layer architectures for use in both negative and positive electrodes are developed through a layer-by-layer spray printing approach using complementary material combinations, with the ultimate goal to realize an ideal concept of hybrid lithium-ion capacitors more fully – delivering attractive energy densities of insertion-type negative electrodes while preserving outstanding power performances of activated carbon positive electrodes. To sustain advantageous capacities of intercalation anodes even at ultra-fast charging rates, a thin, discrete layer of high capacity Si was interleaved between high power $Li_4Ti_5O_{12}$ electrodes. In a cathode electrode, a sequential layer of insertion-type $LiFePO_4$ was assembled with a conventional activated carbon layer into a single layer structure, aiming at boosting overall deliverable capacities. The lithium-ion capacitor comprising the smart multi-layer architectures of negative and positive electrodes then provided a remarkable energy density of ~110 Wh/kg with an outstanding power performance of 15 kW/kg.

A lithium-ion capacitor (LIC) is a hybrid of a lithium-ion battery (LIB) and an electrochemical capacitor (EC), aiming to improve energy density of ECs comparable with that of LIBs (300–400 Wh/kg) while sustaining fascinating power capability of ECs (2–10 kW/kg).[1–3] However, realizing both high energy and high power density in a single LIC configuration may be hard-to-achieve in practice because of a rapid capacity collapse of a insertion-type negative electrode at ultra-fast charging rates and intrinsically low energy density of the electrical double layer (EDL)-based activated carbon (AC) on a positive electrode side.[4–6]

From an electrode material point of view, high capacity negative electrode materials including Si, Ge and SnO_2 have a potential to promote overall LIB capacity even at increasing rates if problematic volume expansion of these materials during intercalation processes is controllable appropriately in a proper manner, which can offer superior rate capability over conventional graphite-based materials.[7,8] On the other hand, the hybridization of capacitive AC with optimized insertion-type battery materials (e.g., $LiFePO_4$, $LiCoO_2$ or $LiMnO_2$) shows promise for boosting an inherently low capacity of EC electrodes.[9,10] To investigate a new capacity-power combination in LIC configurations, it is significant to develop an effective processing approach that can incorporate advantageous attributes of such active materials into both negative and positive electrodes by optimizing compositions and spatial distribution of constituents within electrode microstructures.

We have recently developed a new type of electrode architectures, particularly by exploiting a relatively unexplored manufacturing approach "spray coating" that provides a flexibility in electrode designs to create extra performance benefits and functionality, unavailable by a conventional slurry casting method.[11,12] For instance, a bespoke multi-layer electrode was designed by spray coating of discreate layers of high capacity Si and high power $Li_4Ti_5O_{12}$ (LTO), layer-by-layer, in a recent publication.[13] Careful optimization on multi-layer structures and performances, for example by varying the thickness of discrete Si in the range of 2 to 8 μm (5 to 20 wt%), provided that a thinner Si was most effective to tolerate accelerated, continuous intercalation strains at increasing charge/discharge rates and over cycles. The best location of the best performing 2 μm Si within the through-thickness multi-layer was then explored, suggesting that locating the Si layer closer to the separator/positive electrode (reversely further away from the current collector), in principle, allows for the shortest pathway for active ions traveling towards and from high capacity Si, and thus is advantageous in terms of lithiation reaction kinetics. Currently, hybrid electrode structures were also developed by spray coating of capacitive AC (YP-50F, YP) and insertion-type $LiFePO_4$ (LFP) into otherwise multi-layers.[14] Performance balances between power (YP) and capacity (LFP) were then thoroughly studied as a function of weigh fractions and spatial variations of discrete LFP layers, with the intention to take best advantage of composite electrode designs that outperform a configuration with LFP "randomly scattered" across YP.

In this research, the best combination of LTO-Si and LFP-YP was now explored to realize the inherent multi-layering benefits more fully in a single LIC format. For example, a thin, discrete Si (~5 wt%) layer was spray deposited on a pre-formed LTO layer, whereas advantageous LFP (~20 wt%) was stacked over a traditional YP electrode. The arising multi-layer architectures were then coupled together into a LIC configuration as negative and positive electrodes, respectively. Apart from the multi-layer arrangement, various types of LIC configurations were also prepared by otherwise identical spray coating in order to investigate and compare the energy-to-power balance:

[a] Prof. Dr. S. H. Lee
Department of Chemical Engineering
Pukyong National University
45 Yongso-ro, Nam-gu, 48513, Busan, South Korea
E-mail: sangho.lee@pknu.ac.kr

Supporting information for this article is available on the WWW under https://doi.org/10.1002/batt.202200380

Research Article
doi.org/10.1002/batt.202200380
Chemistry Europe
European Chemical Societies Publishing

(i) LTO-only || YP-only, (ii) LTO-only || LFP-YP, (iii) LTO-Si || YP-only and (iv) LTO-Si || LFP-YP. The LTO-Si || LFP-YP then provided a marked energy density of ~110 Wh/kg at 0.1 C and a power density of 15 kW/kg at 300 C that outperformed a conventional LIC in terms of power and capacity.

Results and Discussion

Figure 1 schematically depicts the fabrication of multi-layer architectures using a layer-by-layer spray coating process. There are three key requirements to ensure the successful multi-layer fabrication. The first factor is to use a fugitive bi-solvent mixture of deionized (DI) water and isopropyl alcohol (IPA) for the spray suspension. Here, IPA helps to disperse conductive carbon into the aqueous solution,[15,16] allowing for successive pumping of suspension and atomization into liquid droplets at the nozzle without pulsing. The second thing is to use a heated current collector that is pre-set to a temperature higher than the boiling point of both DI and IPA. The use of the heated current collector results in the fast, effective drying of deposited suspension droplets over the pre-formed sub-layer, enabling the layer-by-layer formation of discrete layers into a single multi-layer configuration, as described in the scheme in Figure 1. Furthermore, a high degree of freedom in a multi-layer design is achievable simply by switching between feedstock suspension types at will. The last one is the reciprocating motion of the spray nozzle over the heated current collector. The cone-shaped spray of the atomized suspension moves repetitively in a pre-programmed zig-zag pattern in the *x* and *y* plane with a fixed *z* spray distance, leading to the precise control over electrode thicknesses by modifying the number of spray scan cycles. The effective electrode area is modified as a function of variations in the range of nozzle motion.

We utilized useful combinations of complementary materials to boost both power and energy densities in a LIC configuration. For example, while a multi-layer negative electrode of high capacity Si and high power LTO was exploited to enhance LIC rate capability, a hybrid positive electrode of insert-type LFP and capacitive YP was employed to promote LIC deliverable capacities. Figures 2a and 2b show scanning electron microscope (SEM) images for the cross-sections of the spray printed LTO-only electrode and the spray coated multi-layer of LTO and Si (denoted as LTO-Si), respectively. For the multi-layer fabrication, a thick LTO layer (~27 μm) was spray coated first over the Cu current collector, and then a relatively thin Si layer (~3 μm) was consecutively deposited on the pre-formed LTO (Figure S1 in the Supporting Information provides magnified images at the junction between discrete layers of LTO and Si and between LTO and the Cu current collector). Note that the LTO-only electrode thickness was also maintained at ~30 μm in order to compare electrochemical performances of the arising LTO-Si multi-layer. Figure 2(c and d) shows corresponding energy-dispersive X-ray spectroscopy (EDS) element map images for Ti (yellow) and Si (red) within the through-thickness LTO-Si multi-layer, respectively. SEM images

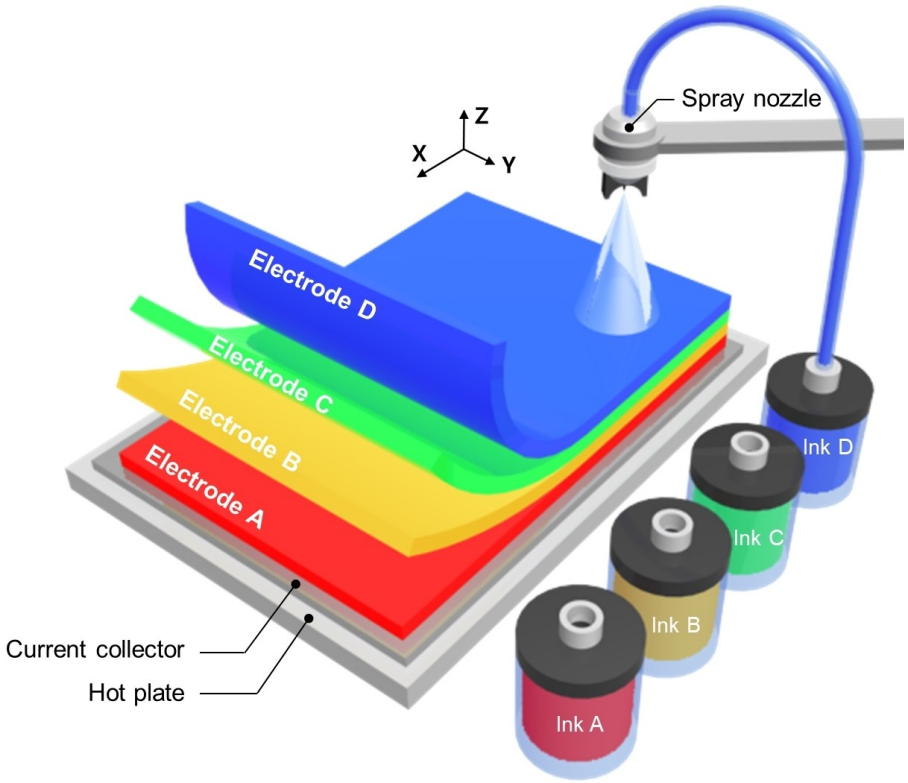

Figure 1. Graphical illustration for the fabrication of the multi-layer architecture by spray coating using switching between feedstock suspension types.

Research Article
doi.org/10.1002/batt.202200380
Chemistry Europe
European Chemical Societies Publishing

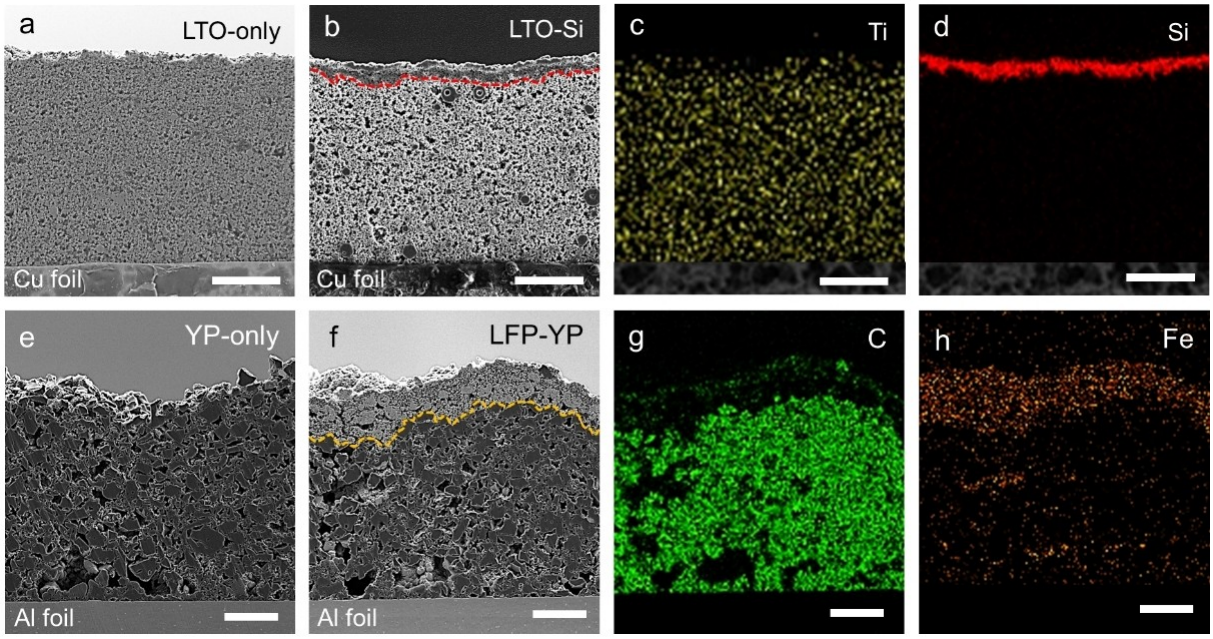

Figure 2. SEM images for the cross-section of a) the LTO-only and b) the LTO-Si electrodes. Before SEM measurements, electrodes were processed using Cross-section & Planar milling system (697 Ilion II, Gatan) in order to ensure the electrode cross-section. Corresponding EDS element map images for c) Ti and d) Si within the LTO-Si multi-layer. SEM images for the cross-section of e) the YP-only and f) the LFP-YP electrodes. Corresponding EDS data for g) C and h) Fe within the LFP-YP multi-layer. All the scale bars indicate 10 μm.

and X-ray diffraction (XRD) patterns in Figure S2 of the Supporting Information characterize detailed structures of pristine particulates of LTO and Si.[17,18]

While Figure 2(e) shows a SEM image for the cross-section of a spray coated 45 μm YP-only electrode, Figure 2(f) presents a hybrid electrode with ~10 μm insertion-type LFP deposited on ~35 μm capacitive YP (LFP-YP) (refer to magnified views for a portion of the junction between active materials of LFP and YP and between YP and the Al current collector in Figure S3 of the Supporting Information), both of which were made to be utilized as LIC positive electrodes. Figure 2(g and h) represents EDS map images for C (green) and Fe (orange), respectively. It supports that two layers of YP and LFP remain continuous and discrete, even with some unwanted contamination that may be caused by the pre-treatment using Ar beam in order to secure nice cross-sections of the arising electrode. Figure S4 in the Supporting Information provides detailed structures for pristine particulates of YP and LFP.[19]

Figure 3 exhibits a series of half-cell performance data for the four electrodes: LTO-Si, LTO-only, YP-LFP and YP-only. Figure 3(a) represents cyclic voltammetry (CV) curves for the LTO-Si and LTO-only negative electrodes, presenting a pair of anodic/cathodic peak densities at 1.75 and 1.5 V, respectively, characteristics of spinel LTO. In the inset, the magnified CV profiles show additional strong anodic/cathodic peak current densities at approximately 0.5 and 0.4 V only for the LTO-Si multi-layer (red), which were associated with lithium intercalations on Si.[20,21] Figure S5(a) in the Supporting Information also presents comparative CV plots including the Si-only electrode (blue). Figure 3(b) shows the gravimetric discharge capacity profiles at increasing rates of 10 to 2000 mA/g for the LTO-Si and LTO-only electrodes. The LTO-Si multi-layer outweighed the LTO-only electrode in terms of discharge capacities at all rates. Particularly, at 2000 mA/g the LTO-Si multi-layer had a discharge capacity of ~200 mAh/g, twice that of the LTO-only equivalent (~100 mAh/g), given in Table 1. The right corner inset represents comparative charge/discharge curves in the 1st cycle, showing a much longer plateau at approximately 0.3 V for the LTO-Si electrode (red) that was associated with the well-known solid electrolyte interface (SEI) formation on Si. Also, the LTO-Si multi-layer were compared with the spray printed Si-only electrode to investigate advantageous characteristics of the layering approach, as shown in the bar graph in Figure S6 of the Supporting Information. While extraordinarily high

Table 1. Summary of data for the spray coated LTO-only, LTO-Si, YP-only and LFP-YP electrodes.

Electrode type	Loading mass [mg/cm^2]	Thickness [μm]	Half-cell capacity [mAh/g] 10 mA/g	100 mA/g	1 A/g	2 A/g
LTO-only	3.02 ± 0.02	30 ± 2	230	195	120	100
95 wt% LTO + 5 wt% Si	3.04 ± 0.02	31 ± 4	320	245	220	200
YP-only	3.03 ± 0.02	45 ± 5	40	35	25	20
80 wt% YP + 20 wt% LFP	3.02 ± 0.03	44 ± 3	60	55	45	35

Research Article
doi.org/10.1002/batt.202200380
Chemistry Europe
European Chemical Societies Publishing

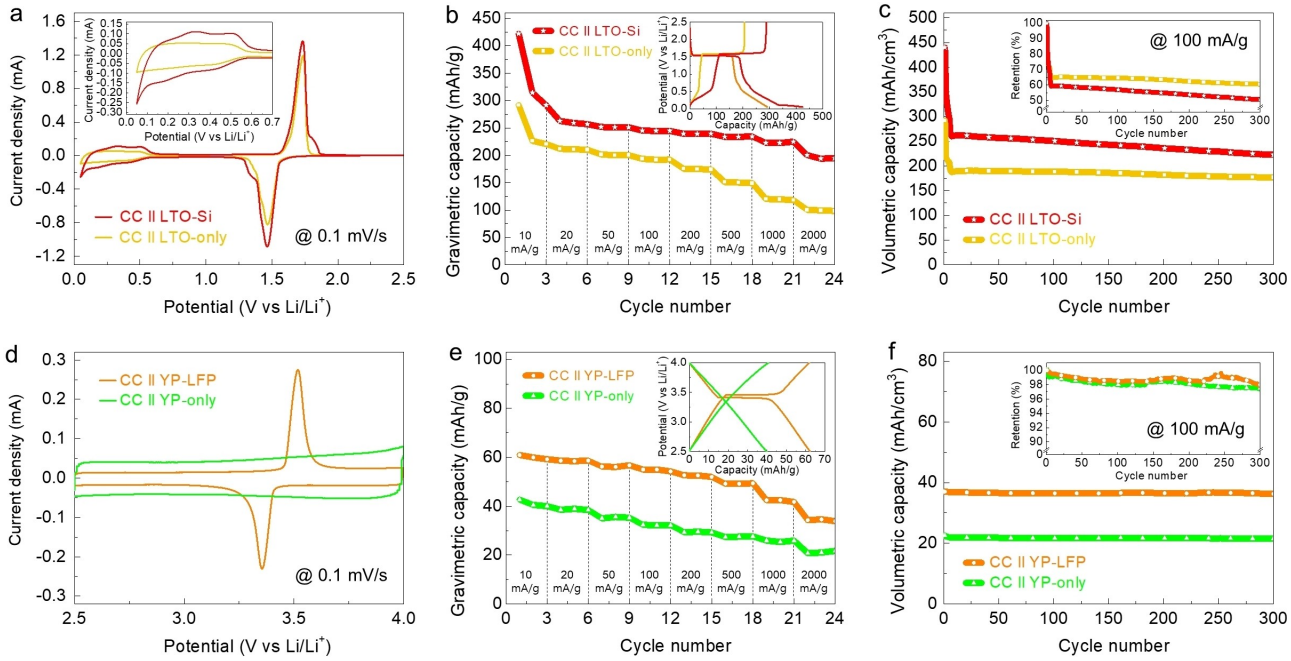

Figure 3. a) CV curves of the LTO-Si and LTO-only electrodes at a constant scan rate of 0.1 mV/s in the potential range 0.05 to 2.5 V (vs. Li/Li^+). The inset magnifies the CV plots in the potential range 0.0 to 0.7 V (vs. Li/Li^+). b) Gravimetric discharge capacity profiles at increasing rates in the potential range 0.05 to 2.5 V (vs. Li/Li^+). The inset shows gravimetric charge/discharge plots at 20 mA/g in the potential range 0.05 to 2.5 V (vs. Li/Li^+). c) Volumetric discharge capacity profiles at 100 mA/g in the voltage window 0.05 to 2.5 V (vs. Li/Li^+) and the corresponding capacity retention profiles (inset). d) CV curves of the LFP-YP and YP-only electrodes at 0.1 mV/s in the potential range 2.5 to 4.0 V (vs. Li/Li^+). e) Gravimetric discharge capacity plots at increasing rates in the potential range 2.5 to 4.0 V (vs. Li/Li^+). The inset indicates gravimetric charge/discharge plots at 20 mA/g in the potential range 2.5 to 4.0 V (vs. Li/Li^+). f) Volumetric discharge capacity profiles at 100 mA/g in the voltage window 2.5 to 4.0 V (vs. Li/Li^+) and the corresponding capacity retention profiles (inset).

capacities of the Si-only electrode at low rates collapsed catastrophically as current densities increased to 2000 mA/g, the LTO-Si multi-layer delivered attractively high discharge capacities even at 1000 mA/g and 2000 mA/g that outperformed the LTO-only and Si-only electrodes, given in Table S1 of the Supporting Information. Figure 3(c) shows galvanostatic discharge capacity profiles at a constant rate of 100 mA/g for the same electrodes. After 300 cycles, the LTO-Si multi-layer retained a volumetric discharge capacity of ~220 mAh/cm^3, showing an approximately 25% improvement in a deliverable capacity when compared with the LTO-only electrode (~180 mAh/cm^3). Here, the volumetric capacity values were estimated by normalizing the resulting gravimetric capacities by the loading mass and thickness of the electrodes, as given in Table 1. The right corner inset shows the corresponding capacity retention after 300 cycles, indicating ~50% and ~60% capacity retention for the LTO-Si and LTO-only electrodes, respectively. The relatively severe capacity degradation of the LTO-Si was as expected due to side reactions on Si including continuous SEI formation and volume expansion as charge/discharge cycles progressed repeatedly, whereas an initially low capacity of the LTO-only electrode was well sustained up to the 300th cycle.

As a counterpart in LIC arrangements, Figure 3(d) shows CV profiles at a constant scan rate of 0.1 mV/s for the LFP-YP and YP-only positive electrodes. As a thin layer of LFP was interleaved between the YP-based multi-layers, the anodic/cathodic peak currents at approximately 3.5 V (the anodic sweep) and 3.3 V (the cathodic sweep) increased markedly, and EDL thicknesses decreased correspondingly, implying that energy storage mechanism of the LFP-YP hybrid electrode was associated with both the EDL mechanism (YP) and the intercalation reaction (LFP). Figure 3(e) shows the gravimetric discharge capacity profiles at increasing rates of 10 to 2000 mA/g for the same electrodes. The LFP-YP hybrid electrode overwhelmed the YP-only equivalent in terms of deliverable discharge capacities at all rates, supporting an insight that the intercalation reaction from LFP was useful to overcome an intrinsically low energy density of traditional YP electrodes (Figure S8 and Table S2 in the Supporting Information show comparative half-cell performances for the LFP-only, YP-only and LFP-YP electrodes). The right corner inset presents gravimetric charge/discharge profiles at 20 mA/g. While the YP-only electrode showed a linear response, typical of the EDL charge storage mechanism, the LFP-YP multi-layer had long voltage plateaus between 3.3 to 3.5 V, again showing the involvement of the intercalation mechanism of LFP. Figure 3(f) shows galvanostatic discharge capacity profiles at 100 mA/g. After 300 cycles, the YP-only and LFP-YP multi-layer electrodes sustained volumetric discharge capacities of ~40 mAh/cm^3 and ~20 mAh/cm^3, respectively, both of which had ~98% capacity retention, as shown in the upper inset.

The performance benefits of multi-layer architectures were then explored in full LIC configurations. To identify the best combination of negative and positive electrodes that can provide the best capacity-power response, LICs were assembled

Research Article
doi.org/10.1002/batt.202200380
Chemistry Europe
European Chemical Societies Publishing

with various types of negative and positive electrodes: (i) LTO-only || YP-only, (ii) LTO-Si || YP-only, (iii) LTO-only || LFP-YP and (iv) LTO-Si || LFP-YP. Figure 4(a) shows comparative energy density retention profiles at increasing C-rates for the four LIC configurations. At relatively low rates of 0.1 to 5 C, LIC types comprising LFP-YP positive electrodes had superior energy density over LICs using YP-only equivalents, implying that the balanced LFP intercalation capacity contributed markedly to improvements in overall LIC energy density at low rates. As C-rates increased further to 300 C, LICs assembled with LTO-Si negative electrodes retained much higher energy density than LICs with LTO-only equivalents. Given that fast-charging attributes of LICs tend to be constrained by a relatively fast capacity degradation and sluggish reaction kinetics of insertion-type negative electrodes, interleaving a discrete layer of large volume expansion Si between zero-strain insertion LTO layers and locating kinetically advantageous Si closest to a positive electrode were shown to result in marked improvements in overall LIC power performances. Consequently, the LIC configuration of LTO-Si || LFP-YP had the highest performances, with ~110 Wh/kg at 0.1 C and ~15 kW/kg at 300 C that correspond to almost 300% improvements in both the energy and power density when compared with the usual LTO || YP combination (~45 Wh/kg and ~5 kW/kg at the same conditions). The inset shows comparative charge/discharge curves for the identical LIC configurations. LICs using YP-only electrodes (green and blue) showed a linear charge/discharge response,[22,23] whereas voltage plateaus appeared apparently at around 1.8 V as LFP was incorporated into positive electrodes (red and yellow). The plateaus then became longer by adding a discrete Si layer into a LIC negative electrode (red). Capacitance could be estimated using $C = i \times t/V$ [F/g], where i is the applied current density [A/g], t is the discharge or charge time [s], and V is the potential difference [V].[24,25] At 2.5 A/g, the LTO-Si || LFP-YP configuration delivered the highest capacitance of ~110 F/g that was almost three times that of a conventional LTO || YP (~40 F/g). The LTO-Si || YP-only and LTO-only || LFP-YP had ~85 F/g and ~75 F/g at the same rate, respectively.

The best performing LTO-Si || LFP-YP was also compared with other LIC configurations in recent literatures that comprised LTO negative electrodes and AC positive electrodes, as shown in comparative Ragone plots in Figure 4(b).[26–32] The LTO-Si || LFP-YP configuration outweighed, or at least, was comparable with other LICs in terms of both energy and power densities, although many of competing LIC performances were shown to rely on comparatively higher fractions of conductive carbon enhancers and polymeric binders (≥20 wt%) that were utilized to enhance overall LIC performances. Please note that all LIC electrodes used in this research were manufactured with

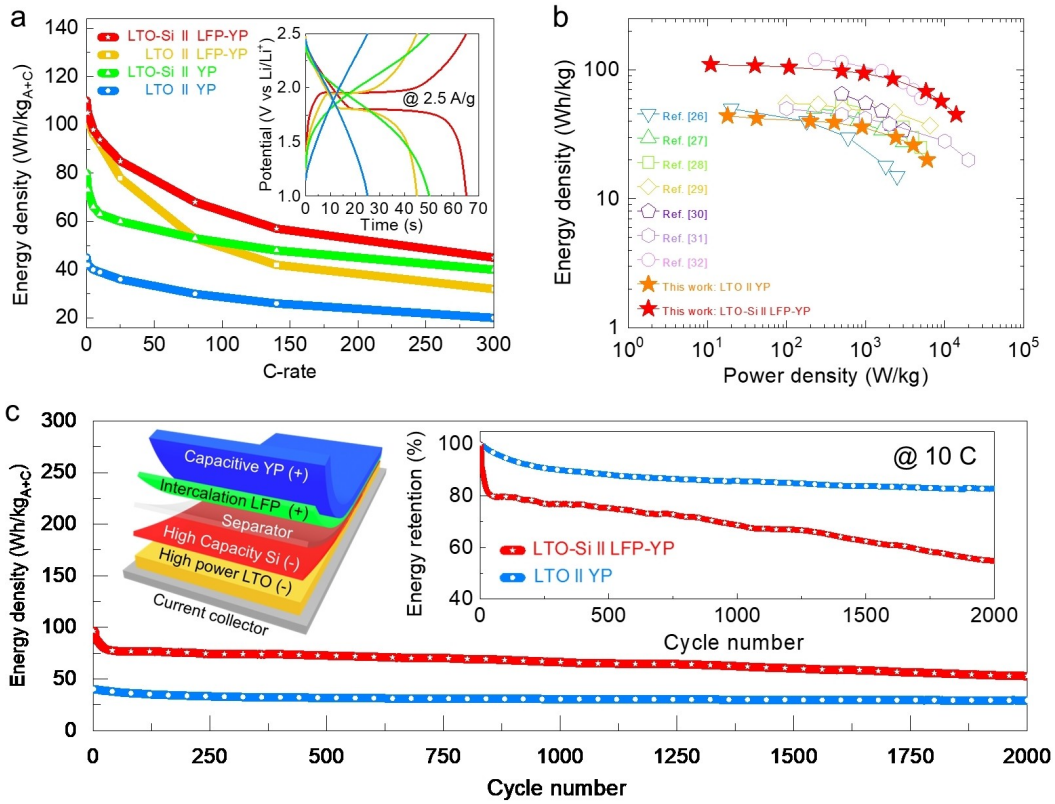

Figure 4. a) Gravimetric discharge energy density profiles as a function of C-rates in the potential range 1.0 to 2.5 V (vs. Li/Li$^+$) for LIC configurations of LTO-Si || LFP-YP, LTO-only || LFP-YP, LTO-Si || YP-only and LTO-only || YP-only. The inset indicates gravimetric charge/discharge curves at 2.5 A/g in the potential range 1.0 to 2.5 V (vs. Li/Li$^+$) for the identical LICs. b) Comparative Ragone plots as a function of LIC configurations. c) Galvanostatic discharge energy density profiles at 10 C in the voltage window 1.0 to 2.5 V (vs. Li/Li$^+$) and the corresponding energy density retention profiles (the right-hand inset). The left-hand inset depicts the combination of LTO-Si and LFP-YP electrodes within a full LIC arrangement.

Research Article
doi.org/10.1002/batt.202200380
Chemistry Europe
European Chemical Societies Publishing

Table 2. Summary data for spray coated negative and positive electrodes in full LIC configurations.

LIC type	Electrode loading mass [mg/cm^2]		Electrode thickness [μm]			
	Anode	Cathode	Anode		Cathode	
			LTO	Si	LFP	YP
LTO ‖ YP	3.02 ± 0.02	9.07 ± 0.03	30 ± 1	0	0	103 ± 4
LTO-Si ‖ YP	3.04 ± 0.03	9.09 ± 0.05	27 ± 2	3 ± 1	0	104 ± 5
LTO ‖ LFP-YP	3.01 ± 0.03	9.07 ± 0.05	31 ± 1	0	20 ± 3	78 ± 3
LTO-Si ‖ LFP-YP	3.03 ± 0.02	9.08 ± 0.04	28 ± 2	3 ± 1	21 ± 2	77 ± 4

a small fraction of inactive constituents (~5 wt%) that incur weight and volume penalties to the LIC capacity estimation.

Figure 4(c) shows the galvanostatic discharge energy density profiles at 10 C for the LTO-Si ‖ LFP-YP and LTO-only ‖ YP-only arrangements. After 2000 cycles, the LTO-Si ‖ LFP-YP retained a discharge energy density of ~55 Wh/kg that was almost double that of the LTO-only ‖ YP-only (~30 Wh/kg). The right-hand inset shows that the LTO-Si ‖ LFP-YP configuration had comparatively lower energy density retention (~55%) than the LTO-only ‖ YP-only equivalent (~80%) at the 2000th cycle. This is likely because of a relatively fast decline in the initially energy density that was associated with repetitive SEI formation and harmful volume expansion on Si at an ultra-fast rate of 10 C and over continuous charge/discharge cycles,[33,34] which may be potentially overcome through improving electrode material aspects, e.g., by surface coating of Si with soft carbons[35–37] or by exploiting a wide range of buffering designs, including core-shell structures, hollow frameworks or hierarchical configurations.[38–40] The left-hand inset represents a scheme for the LTO-Si ‖ LFP-YP LIC configuration.

Conclusion

The capability and limitation of multi-layer architecture electrodes for LIC applications were explored by exploiting complementary material combinations, e.g., high power LTO and high capacity Si in negative electrodes and conventional YP and unconventional LFP in positive electrodes, respectively. Initially, the electrochemical behaviors of the arising multi-layers were investigated in half-cell configurations, aiming to understand the fundamental energy storage mechanism of the multi-layer architecture. The best combination of the LTO-Si ‖ LFP-YP then led to an attractive energy density of ~110 Wh/kg and an outstanding power density of 15 kW/kg in full LICs.

The bespoke multi-layering approach could be a cutting-edge technology in the electrode manufacture that can be expected to supply an optimum quantity of electrode constituents at the right place where betterfunctionality or more effective material utilization is required, leading to extra performance benefits in overall cell capacity and power.

Experimental Section

Materials. LTO and CMC were obtained from Sigma Aldrich; Si from Alfa Aesar; YP from Kuraray; LFP and SP from MTI.

Spray coating process. For the suspension, active materials (LTO, Si, YP or LFP), SP and CMC in a controlled mass ratio of 95:3:2 were suspended into a mixture of DI water and IPA using ultrasonication. The suspension concentration was approximately 5 mg/mL for the fabrication of both anode and cathode electrodes. Prior to the spray coating, the current collect (e.g., Cu, Al or stainless steel) was fixed on a vacuum chuck of a hot plate that was pre-set at a constant temperature of 110 °C, so that local pore fractions and resulting performances of electrodes were retained consistently. The prepared suspension was then pumped to the spray nozzle and subsequently atomized under a controlled air pressure of 0.3 to 0.5 bar. All spray processes were carried out in a well-ventilated fume cupboard.

Electrochemical tests. Electrochemical performances of spray printed electrodes were investigated using coin-type cells (CR2032, MTI) that were assembled from thoroughly dried electrodes in an Ar-filled glovebox ($H_2O < 0.1$ ppm, $O_2 < 0.1$ ppm, KOREA KIYON). For half-cell tests, working electrodes were coupled with pure lithium chips (99.9% trace metals basis, MTI) that were used as a counter/reference electrode. For LIC cells, spray printed negative electrodes (e.g., LTO-only or LTO-Si) were paired with spray printed positive electrodes (e.g., YP-only or LFP-YP). Negative and positive electrodes were electrically separated by a 25 μm polypropylene separator (Celgard 2400) that was soaked into 1 M $LiPF_6$ electrolyte solution in a 1:1 mixture (by volume) of ethylene carbonate and dimethyl carbonate (Sigma-Aldrich). All LICs were formulated with a 1:3 anode:cathode mass ratio, given in Table 2. Charge/discharge measurements were conducted at room temperature using WonATech battery cyclers (WBCS3000 L). While half-cell capacities were calculated based on the total electrode mass including active materials (LTO, Si, YP or LFP), SP and CMC, full LIC performances were estimated using the total mass of negative and positive electrodes. CV measurements were carried out using Autolab M204. The theoretical capacity of LTO, Si and LFP was assumed to be ~175 mAh/g,[41] ~4000 mAh/g[13] and ~170 mAh/g,[14] respectively.

Acknowledgements

This work was supported by a Research Grant of Pukyong National University (2021).

Conflict of Interest

The authors declare no conflict of interest.

Data Availability Statement

The data that support the findings of this study are available from the corresponding author upon reasonable request.

Keywords: architecture electrode · capacity-power balance · lithium-ion capacitor · multi-layering · spray printing

[1] A. Jagadale, X. Zhou, R. Xiong, D. P. Dubal, J. Xu, S. Yang, *Energy Storage Mater.* **2019**, *19*, 314.
[2] J. Ding, W. Hu, E. Paek, D. Mitlin, *Chem. Rev.* **2018**, *118*, 6457.
[3] X. Yu, C. Zhan, R. Lv, Y. Bai, Y. Lin, Z. -H Huang, W. Shen, X. Qiu, F. Kang, *Nano Energy* **2015**, *15*, 43.
[4] S. H. Lee, C. Johnston, P. S. Grant, *ACS Appl. Mater. Interfaces* **2019**, *11*, 37859.
[5] X. Zhou, L. Yu, X.-Y. Yu, X. W. Lou, *Adv. Energy Mater.* **2016**, *6*, 1601177.
[6] E. Zhao, C. Qin, H.-R. Jung, G. Berdichevsky, A. Nese, S. Marder, G. Yushin, *ACS Nano* **2016**, *10*, 3977.
[7] S. H. Lee, K. Li, C. Huang, J. D. Evans, P. S. Grant, *ACS Appl. Mater. Interfaces* **2019**, *11*, 603.
[8] N. Liu, H. Wu, M. T. McDowell, Y. Yao, C. Wang, Y. Cui, *Nano Lett.* **2012**, *12*, 3315.
[9] A. Shellikeri, S. Yturriaga, J. S. Zheng, W. Cao, M. Hagen, J. A. Read, T. R. Jow, J. P. Zheng, *J. Power Sources* **2018**, *392*, 285.
[10] B. Wang, Q. Wang, B. Xu, T. Liu, D. Wang, G. Zhao, *RSC Adv.* **2013**, *3*, 20024.
[11] Y. Lu, L. Yu, M. Wu, Y. Wang, X. W. Lou, *Adv. Mater.* **2018**, *30*, 1702875.
[12] Y. Lu, J. Nai, X. W. Lou, *Angew. Chem. Int. Ed.* **2018**, *57*, 2899.
[13] S. H. Lee, C. Huang, P. S. Grant, *Nano Energy* **2019**, *61*, 96.
[14] S. H. Lee, C. Huang, P. S. Grant, *Energy Storage Mater.* **2020**, *33*, 408.
[15] Y. S. Park, J. Jeong, Y. Noh, M. J. Jang, J. Lee, K. H. Lee, D. C. Lim, M. H. Seo, W. B. Kim, J. Yang, S. M. Choi, *Appl. Catal. B* **2021**, *292*, 120170.
[16] S. H. Lee, A. Mahadevegowda, C. Huang, J. D. Evans, P. S. Grant, *J. Mater. Chem. A* **2018**, *6*, 13133.
[17] W. Chen, H. Jiang, Y. Hu, Y. Dai, C. Li, *Chem. Commun.* **2014**, *50*, 8856.
[18] J. Kim, S. Y. Kim, C.-M. Yang, G. W. Lee, *Sci. Rep.* **2019**, *9*, 13313.
[19] X. Xi, G. Chen, Z. Nie, S. He, X. Pi, X. Zhu, J. Zhu, T. Zuo, *J. Alloys Compd.* **2010**, *497*, 377.
[20] S. Guo, X. Hu, Y. Hou, Z. Wen, *ACS Appl. Mater. Interfaces* **2017**, *9*, 42084.
[21] J.-I. Lee, Y. Ko, M. Shin, H.-K. Song, N.-S. Choi, M. G. Kim, S. Park, *Energy Environ. Sci.* **2015**, *8*, 2075.
[22] S. H. Lee, C. Johnston, P. S. Grant, *Energy Technol.* **2020**, *8*, 2000253.
[23] S. H. Lee, C. Huang, P. S. Grant, *Energy Storage Mater.* **2021**, *38*, 70.
[24] Y. Sun, J. Tang, F. Qin, J. Yuan, K. Zhang, J. Li, D.-M. Zhu, L.-C. Qin, *J. Mater. Chem. A* **2017**, *5*, 13601.
[25] C. Huang, J. Zhang, H. J. Snaith, P. S. Grant, *ACS Appl. Mater. Interfaces* **2016**, *8*, 20756.
[26] H. Kim, K.-Y. Park, M.-Y. Cho, M.-H. Kim, J. Hong, S.-K. Jung, K. C. Roh, K. Kang, *ChemElectroChem* **2014**, *1*, 125.
[27] H. Xu, X. Hu, Y. Sun, W. Luo, C. Chen, Y. Liu, Y. Huang, *Nano Energy* **2014**, *10*, 163.
[28] D. Puthusseri, V. Aravindan, S. Madhavi, S. Ogale, *Electrochim. Acta* **2014**, *130*, 766.
[29] Y. Lei, Z.-H. Huang, Y. Yang, W. Shen, Y. Zheng, H. Sun, F. Kang, *Sci. Rep.* **2013**, *3*, 2477.
[30] A. Jain, V. Aravindan, S. Jayaraman, P. S. Kumar, R. Balasubramanian, S. Ramakrishna, S. Madhavi, M. P. Srinivasan, *Sci. Rep.* **2013**, *3*, 3002.
[31] Y. Chikaoka, E. Iwama, T. Ueda, N. Miyashita, S. Seto, M. Sakurai, W. Naoi, M. T. H. Reid, P. Simon, K. Naoi, *J. Phys. Chem. C* **2020**, *124*, 12230.
[32] Y.-T. Lin, C.-W. Chang-Jian, T.-H. Hsieh, J.-H. Huang, H. C. Weng, Y.-S. Hsiao, W.-L. Syu, C.-P. Chen, *Appl. Surf. Sci.* **2021**, *543*, 148717.
[33] M.-S. Wang, W.-L. Song, L.-Z. Fan, *ChemElectroChem* **2015**, *2*, 1699.
[34] M. Dirican, Y. Lu, K. Fu, H. Kizil, X. Zhang, *RSC Adv.* **2015**, *5*, 34744.
[35] Y. Liu, J. Liu, M. Hou, L. Fan, Y. Wang, Y. Xia, *J. Mater. Chem. A* **2017**, *5*, 10902.
[36] X. Guo, C. Wang, M. Chen, J. Wang, J. Zheng, *J. Power Sources* **2012**, *214*, 107.
[37] K. Zhang, J.-T. Lee, P. Li, B. Kang, J. H. Kim, G.-R. Yi, J. H. Park, *Nano Lett.* **2015**, *15*, 6756.
[38] P. Li, J. Y. Jeong, B. Jin, K. Zhang, J. H. Park, *Energy Storage Mater.* **2020**, *25*, 687.
[39] H. Tian, H. Tian, W. Yang, F. Zhang, W. Yang, Q. Zhang, Y. Wang, J. Liu, S. R. P. Silva, H. Liu, G. Wang, *Adv. Funct. Mater.* **2021**, *31*, 2101796.
[40] Y. Yao, M. T. McDowell, I. Ryu, H. Wu, N. Liu, L. Hu, W. D. Nix, Y. Cui, *Nano Lett.* **2011**, *11*, 2949.
[41] S. H. Lee, C. Huang, C. Johnston, P. S. Grant, *Electrochim. Acta* **2018**, *292*, 546.

Manuscript received: August 26, 2022
Revised manuscript received: October 6, 2022
Accepted manuscript online: October 17, 2022
Version of record online: November 18, 2022